

# Tying finger pad skin deformation to tactile perception of object compliance at various time-scales

---

A

Thesis

Presented to

the faculty of the School of Engineering and Applied Science

University of Virginia

---

in partial fulfillment

of the requirements for the degree

Master of Science

by

Bingxu Li

December 2020

## **APPROVAL SHEET**

This  
Thesis  
is submitted in partial fulfillment of the requirements  
for the degree of  
Master of Science

Author: Bingxu Li

Advisor: Gregory Gerling

Advisor:

Committee Member: Gregory Gerling

Committee Member: Reid Bailey

Committee Member: Seongkook Heo

Committee Member:

Committee Member:

Committee Member:

Accepted for the School of Engineering and Applied Science:



Craig H. Benson, School of Engineering and Applied Science

December 2020

## **Abstract**

We regularly touch soft, compliant fruits and tissues. To help us discriminate them, we rely upon cues embedded in spatial and temporal deformation of finger pad skin. However, we do not yet understand, in touching objects of various compliance, how such patterns evolve over time, and thereby drive perception. Prior efforts have focused upon the analysis of finger displacement, reaction force, and 2-D estimates of terminal contact area. However, characterizing the deformation of the skin surface, induced upon contact with compliant surfaces, requires 3-D empirical measurements over a short time-scale, due to its complex nonlinear elasticity and geometry. Herein we couple the empirical measurement of skin deformation – across compliance, indentation depth, indentation rate, and time duration – with human perceptual experiments. In particular, we develop a 3-D stereo imaging technique and metrics for quantifying skin deformation to move 2-D estimates of terminal contact area to 3-D spatiotemporal changes in penetration depth, surface curvature, and force. We observe a complementary interplay between and evolution of these cues over about a 0.3 – 0.6 msec duration at which the stimuli become discriminable, with distinctions between compliances less or more stiff than the skin. We examined the compliance discriminability across slow and fast indentation rates and concluded that the detection rate is higher at slower indentation velocity. Additionally, the minimum time required for differentiating compliance can also be determined psychophysically and biomechanically. These observations of the skin’s deformation may guide the design and control of haptic actuation. Moreover, using our metrics, people can potentially model the skin mechanics of the fingertip and link them to the afferent responses transduced by tactile stimuli.

# Table of Contents

<b>ABSTRACT .....</b>	<b>1</b>
<b>TABLE OF CONTENTS .....</b>	<b>2</b>
<b>LIST OF FIGURES.....</b>	<b>3</b>
<b>LIST OF TABLES.....</b>	<b>3</b>
<b>INTRODUCTION .....</b>	<b>4</b>
<b>RESULTS .....</b>	<b>7</b>
<i>A. PSYCHOPHYSICAL EXPERIMENTS .....</i>	<i>7</i>
<i>B. BIOMECHANICAL EXPERIMENTS.....</i>	<i>9</i>
<i>C. COMPARE COMPLIANCE SENSITIVITY BETWEEN SENSING AND PERCEPTION .....</i>	<i>11</i>
<i>D. RECRUITMENTS OF THE DEVELOPED CUES UNDER FAST AND SLOW INDENTING RATES .....</i>	<i>13</i>
<i>E. METHOD VALIDATION USING CROSS-SECTIONAL CONTOURS.....</i>	<i>15</i>
<i>F. SUMMARY.....</i>	<i>16</i>
<b>METHODS AND MATERIALS.....</b>	<b>17</b>
<i>A. PARTICIPANTS.....</i>	<i>17</i>
<i>B. STIMULI.....</i>	<i>18</i>
<i>C. BIOMECHANICAL EXPERIMENTS.....</i>	<i>19</i>
<i>D. PSYCHOPHYSICAL EXPERIMENTS.....</i>	<i>19</i>
<i>E. DATA ANALYSIS.....</i>	<i>20</i>
1) <i>3-D Surface Reconstruction and Image Processing .....</i>	<i>20</i>
2) <i>Ellipse Method and Image Planes To .....</i>	<i>21</i>
3) <i>Dependent Metrics.....</i>	<i>21</i>
<i>F. STATISTICAL ANALYSIS.....</i>	<i>22</i>
.....	<b>24</b>
<b>DISCUSSION.....</b>	<b>25</b>
<i>A. USABILITY OF THE DEVELOPED CUES.....</i>	<i>25</i>
<i>B. HUMAN DISCRIMINABILITY TO SURFACE COMPLIANCE .....</i>	<i>26</i>
<i>C. CONNECTIONS BETWEEN CUES AND TACTILE AFFERENTS.....</i>	<i>26</i>
<b>REFERENCES .....</b>	<b>28</b>
<b>APPENDIX 1 .....</b>	<b>29</b>
<b>APPENDIX 2 .....</b>	<b>30</b>
<b>APPENDIX 3 .....</b>	<b>43</b>

## List of Figures

<b>Figure 1.</b> Psychophysical evaluation of pairs of compliant stimuli over a range of indentation displacements and velocities. ....	9
<b>Figure 2.</b> Comparison of the four skin deformation cues, evolving over time, between the seven compliant stimuli at slow, medium, and fast rates of indentation. ....	11
<b>Figure 3.</b> Summary of statistical discriminability for each skin deformation cue, for each compliance pair, for each indentation depth and velocity. ....	13
<b>Figure 4.</b> Timeline of the evolution of various cues in the skin’s deformation from about 0.3 to 0.6 seconds. ....	14
<b>Figure 5.</b> A cross-sectional contour representing an example participant’s deformed skin surface is overlaid with points of intersection obtained separately via the ellipse method fitted to the 3-D point cloud. ....	15
<b>Figure 6.</b> Procedure to obtain 3-D point clouds representing the skin deformation at the fingertip while being indented with soft and hard stimuli. ....	24

## List of Tables

<b>Table 1:</b> ANOVA table of stimulus comparisons at 6.5 mm/s indentation velocity at 0.4 s using force cue. ....	23
---	----

## Introduction

Our skin is a deformable, stretchable and sensitive organ with thousands of neural afferents embedded that encode mechanical interactions upon surface contact. People rely on this information to decipher the physical properties of an object, such as compliance, roughness, and shape. Compliance, one attribute within the broad category of softness, stands out because of its importance in a plethora of daily activities, such as inspecting the ripeness of fruit and shaking hands, among others. An object's compliance may also be pleasant and cause us to invite us to touch it. Such compliance may prove crucial in engineering the next generation of cyber physical devices, in particular in coming up with design requirements to empower those engaged in building touch interaction devices and 3-D rendering algorithms [1].

The understanding of compliance is underexplored in terms of physical properties of the skin, neural and psychological responses when a surface is brought into the skin. Due to the complex nonlinear viscoelasticity of the skin's deformation on human's finger pad caused by surface compliance, it remains intricate to model the mechanics of the finger pad. To analyze the geometric change of the skin, previous work proposed a method to measure contact areas by scanning the ink prints after each indentation [2], but this method only provides the terminal contact area without intermediate area changes. More recently, a 3-D image technique was used to generate a point cloud of the finger pad which has potentials to measure the contact area spatially [3] and this paper applies this method.

To interpret the way people interpret compliance psychophysically, Srinivasan and LaMotte (1995) attempted to differentiate the softness of an object with both rigid and deformable surfaces and, the results indicate that perception of softness was most likely caused by the spatiotemporal variation in pressure across the skin surface. They also concluded that solely

cutaneous information is sufficient for passive or tactile touch while people rely on both kinesthetic and tactile cues for active touch [4].

In contrast to our understanding of other aspects of physical properties such as texture and roughness, the neural mechanism underlying the perception of compliance is far less understood. There has been an extensive body of research that focused on the perception of texture by monitoring the afferent responses with various surface microgeometry [5] [6]. When the finger makes contact with a surface, vibrations are elicited and sensed by all tactile afferents and those vibrations were also well studied[7][8]. Yet studies about compliance based on neural responses are very few. Condo and Birznieks (2014) have explored the differential sensitivity to surface compliance by monitoring the afferent's activity such as the spike population and mean firing rate and, the results indicated that the population responses of the slow adapting type I (SAI) showed the greatest sensitivity to compliance. The perceptual ability of compliance, however, and the mechanism of the skin surface still remained unanswered.

Interestingly, most findings from neural models of physical properties such as roughness and compliance indicate complementary roles played by tactile afferents' responses. For example, Johansson and Birznieks found that spiking timing and firing rate of tactile afferent are independent cues to encode the contact surface curvature and force direction. We hypothesis that the empirical measurements of the skin deformation would share similar complementary patterns.

To understand the sensation and perception of compliance, therefore, empirical measurements at the skin-contact surfaces are demanded due to the complexity of mechanism modeling as well as the underexplored afferents' properties. Consequently, the empirical measurements should also reflect the psychophysical responses and neuron activities. In our study, we developed cutaneous cues and tracked the force change to encode the connection between skin

deformation and perception of compliance in passive touch. The developed cues such as penetration depth and curvature are used to quantify the nonlinear deformation of the fingertip and the psychophysical experiments are conducted to track the human perception of compliance. Our work also compared the compliance discriminability at different indentation rates as Srinivasan and LaMotte concluded in their study that indentation velocity has impact on perception of compliance. From the psychophysical experiment conducted via pair-wise stimulus comparison, the minimum time required for compliance differentiation can also be determined. The developed cues also show complementary patterns evolving over different time scales, which agree with the independent nature of tactile afferents' responses discovered by other researchers.

## Results

The aim of our study is to provide empirical measurements of skin deformation when the finger pad making contacts with compliant stimuli, and to compare these measurements with psychophysical responses. A 3-D point cloud that represents the geometry of the finger pad was generated every 100 msec using a disparity-mapping algorithm, and four spatiotemporal cues such as penetration depth and curvature were used to quantify the geometric change of the skin surface. We also conducted psychophysical experiments using pair-wise stimulus comparison to investigate the discriminability of compliance at different indentation rates. In our study, we indented stimuli with different compliance into the participant's index finger at slow and fast indentation velocities. Images of the finger pad from cameras were processed by noise reduction and image processing technique to produce a clean 3-D point cloud, which would be later used for generating metrics using the ellipse method. Since we used displacement control during the experiments, indenting the stimuli up to 1 and 2 mm, the time durations of the loading phase were ranged from 0.3 s to 2 s based on the indentation rates. During the psychophysical experiments, the participants were asked to wear blindfolders to eliminate visual cues and compare the compliance between two stimuli of one pair. The discriminability of compliance was observed by statistical analysis of the developed cues and the psychophysical results, particularly at the same time duration.

*A. Psychophysical experiments.* A total of seven substrates were indented into the participants' index fingers at four indenting rates up to 1 mm displacement, and six rates for 2 mm displacement. Four pairs of stimulus comparison were selected to cover a large range of compliance discriminability as explained in *Methods*. Since all stimulus comparison pairs were

not discriminable at 3.5 mm/s, we did not test any indenting rate beyond that point. The time duration from loading and unloading phases was determined by the indenting rate and displacement. Three levels of time duration (0.3 s, 0.4 s, 0.56 s) were highlighted in Figure 1. As shown, the discriminability of all stimulus pairs decreases as the indenting rates increase. This inverse relationship may result from the reduced time duration during the process. Among the four pairs, 45/10 kPa shows the best discriminability across all the indenting rates, with the highest detection rate of 83% for 1 mm displacement and 100% for 2 mm displacement. On the contrary, 45/75 kPa cannot be differentiated under any circumstances. For the pairs that are both harder and softer than the skin (184/121 kPa and 33/5 kPa), the differentiate sensitivity are almost the same across all indenting rates and displacements. With the threshold of 75% correction rate, the detection time for each pair of stimuli can be determined. The minimum time required to differentiate 45/10 kPa is 0.4 s, 0.56 s for 184/121 kPa and 33/5 kPa and 45/75 kPa can never be differentiated. The change of displacement does not affect the detection time. With the same time duration, the discriminability stays almost the same. Under 0.56 s time duration resulting from 1-mm displacement at 1.75 mm/s and 2-mm displacement at 3.5 mm/s, 45/10, 184/121 and 33/5 kPa have the detection rates of 83%, 76% and 75%, respectively under 1 mm displacement, which are close to the detection rates under 2-mm displacement which are 79%, 78% and 77%. The similar trends shared by 0.4 s and 0.3 s time durations as well.

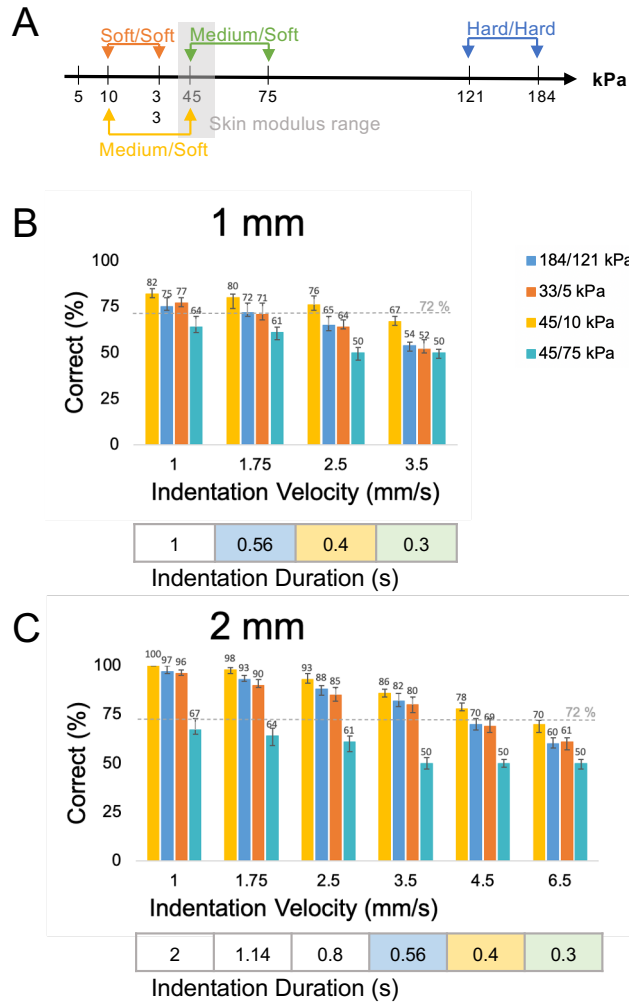


**Figure 1.** Psychophysical evaluation of pairs of compliant stimuli over a range of indentation displacements and velocities.

*B. Biomechanical experiments.* We developed four cutaneous cues to quantify the deformation of the skin surface, which are contact area, penetration depth, force and curvature. For each cue, we plot the magnitude changes over time for seven stimuli, at six indenting rates (see Appendix). For contact area cue, stiffer stimuli result in larger contact areas while the change rate of contact area is more dramatic for the softer stimuli. The duration of the area growth is longer for the softer stimuli compared to the stiffer ones as shown in Figure 2A, that the contact area increased from 20 to 110 mm<sup>2</sup> after 2 s for 5 kPa stimulus while for 184 kPa stimulus, the contact

areas are almost the same after 1 s. Interestingly, the terminal contact area at 1 mm/s for 184 kPa ( $\sim 70 \text{ mm}^2$ ) is smaller than the area at other indenting rates ( $\sim 80 \text{ mm}^2$ ) while other stimuli have almost the same area. One possible explanation for this phenomenon can be the skin relaxation under the slow indentation rate. As indentation rates increase, the differentiability among stimuli decreases along with the time duration. As confirmed by previous studies, softer stimuli have higher penetration depths which still holds for different indenting rates. All stimuli reach to the same level of penetration depth regardless of indentation rates except 1 mm/s which has higher time duration. This means that it takes less time for the skin to get to a certain penetration depth with higher indenting rates. Moreover, soft and hard stimuli are more statistically separated in penetration depth cue than contact area. Force cue shows non-linearity across all indenting rates and substrates, which caused by the non-linear viscoelasticity of the skin surface. All stimuli reach to the similar force level even with the change of indenting rates. The stiffer substrates cause higher magnitude of force which makes it more discriminable compared to softer stimuli. Like the contact area cue, the ultimate curvatures are not influenced by the indenting rates except 184 kPa stimuli at 1 mm/s, which can also potentially be explained by skin relaxation as both the curvature and

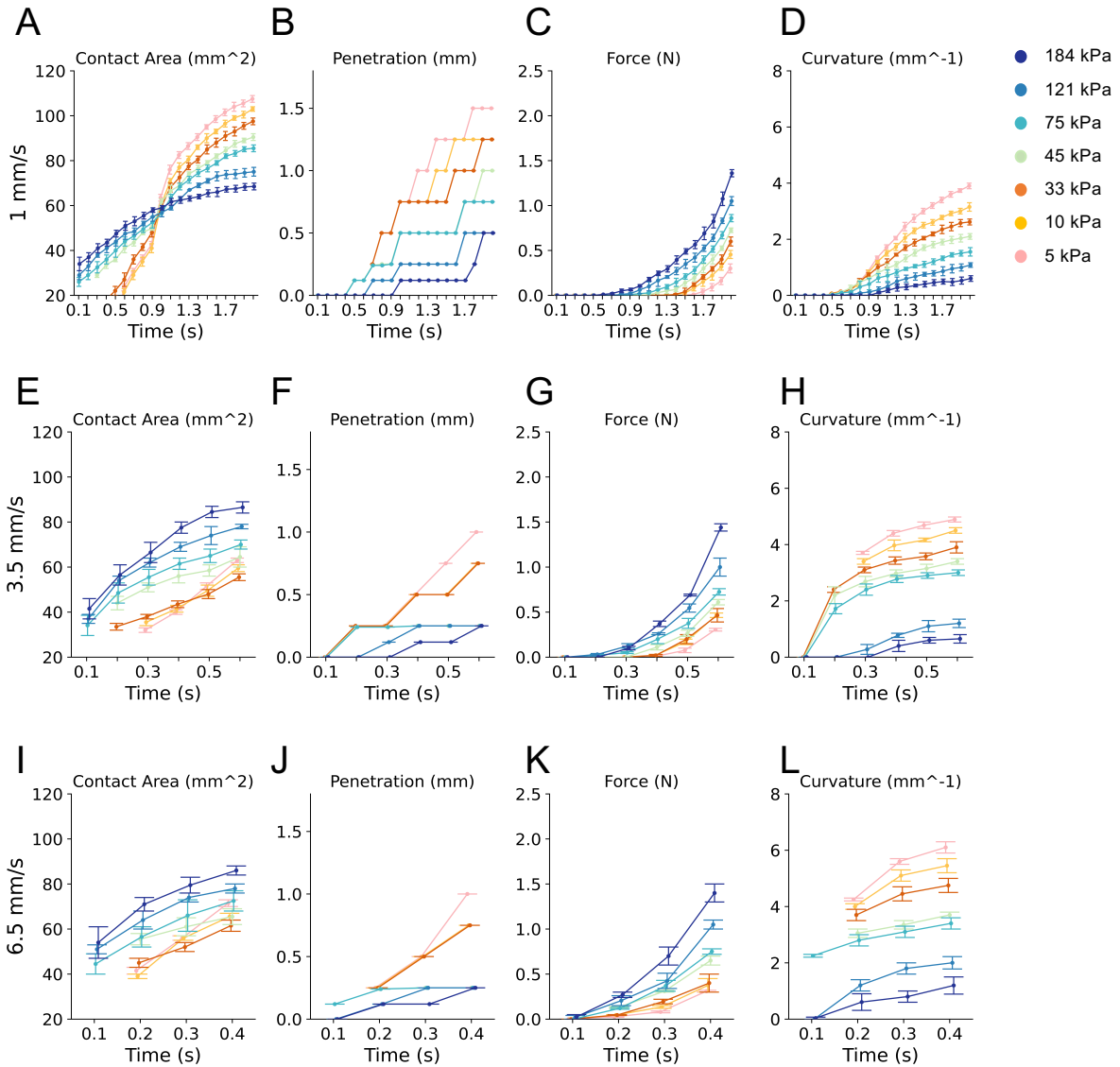


**Figure 2.** Comparison of the four skin deformation cues, evolving over time, between the seven compliant stimuli at slow, medium, and fast rates of indentation.

contact area cue depict the spatial change of the skin. Generally, curvature cue shows the most sensitivity among stimuli and the softer stimuli have higher curvature.

*C. Compare compliance sensitivity between sensing and perception.* The tactile sensing from geometric changes of the skin surface is quantified by the developed cues. The

stimulus pairs with significant difference in between under each cue are presented in the table shown in Figure 3. Apparently, 45/10 kPa is the most distinguishable among other pairs based on the statistics which confirmed the highest detection rate from the psychophysical results. Hard stimulus pair (184/121 kPa) are differentiated earlier than the soft pair (33/5 kPa) using contact area and penetration depth cues shown in Figure 3B, C. Conversely, curvature cue differentiates the soft pair before the hard pair (Figure 3E). Force cue is used exclusively for the hard stimulus pair and at higher indenting rates (Figure 3D). As we also combined the psychophysical results of three levels of time duration highlighted as shaded blocks, we are able to compare the compliance discriminability of each stimulus pair, from the perspectives of skin mechanics and human perception. The comparison shows that the statistical difference does not ensure the perceptual differentiation. For example, 184/121 and 45/10 kPa pairs are statistically differentiable at 6.5 mm/s for all developed cues, whereas neither of them is psychophysically discriminable. Interestingly, for those pairs that can be differentiated by the participants, there are more than one cutaneous cue evolved. People can perceive the difference between 45 and 10 kPa at 3.5 mm/s for example, but they cannot rely on contact area cue in this case. This phenomenon indicates the complementary roles played by the developed cues to help encode differential sensitivity to the surface compliance.



**Figure 3.** Summary of statistical discriminability for each skin deformation cue, for each compliance pair, for each indentation depth and velocity.

*D. Recruitments of the developed cues under fast and slow indenting rates.* In this section, we illustrate the time of each developed cue is recruited. We divide the timeline into three segments as shown in Figure 4 based on the boundary conditions, 0.3 s for 3.5 mm/s and 0.6 s for 6.5 mm/s under 2 mm displacement. Under slow indenting rates, Soft/Soft (S/S) and Medium/Soft (M/S) pairs start to recruit the cues between 0.3 to 0.6 s while Hard/Hard (H/H) pair can be

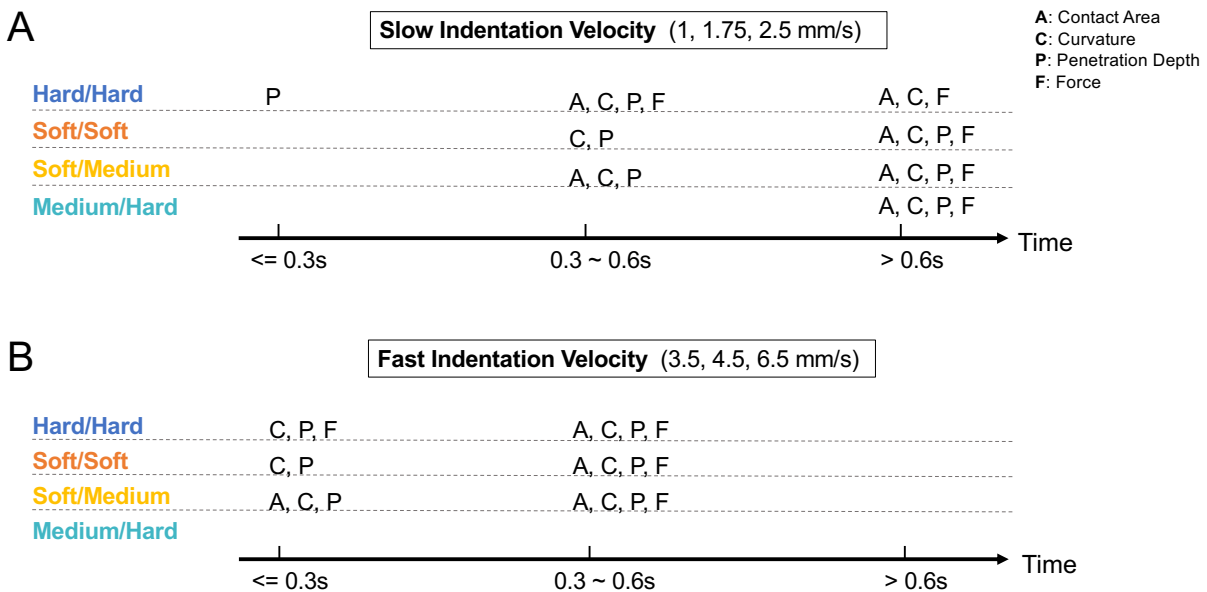


**Figure 4.** Timeline of the evolution of various cues in the skin's deformation from about 0.3 to 0.6 seconds.

differentiated using the penetration cue before 0.3 s. Interestingly, H/H recruits all four cues between 0.3 to 0.6 s but the penetration use is excluded after 0.6 s, while both S/S and M/S have all four cues (Figure 4A). Since faster indenting rates result in shorter time duration, all stimulus pairs except Medium/Hard (M/H) recruit most of the cues before 0.3 s and all four cues are included before 0.6 s (Figure 4B). M/H does not have any recruited cue under fast indenting rates and need more than 0.6 s to include four cues at slow rates. The number of recruited cues is

proportional to the psychophysically discriminability such that longer time duration has more recruited cues which leads to higher detection rates.

*E. Method validation using cross-sectional contours.* We obtain the cross-sectional contours directly from the point clouds before the image processing procedure and impose the image planes from *Ellipse method* along with the developed cues to the contour lines, shown in Figure 5. This representation validates the applied methods visually and statistically as the

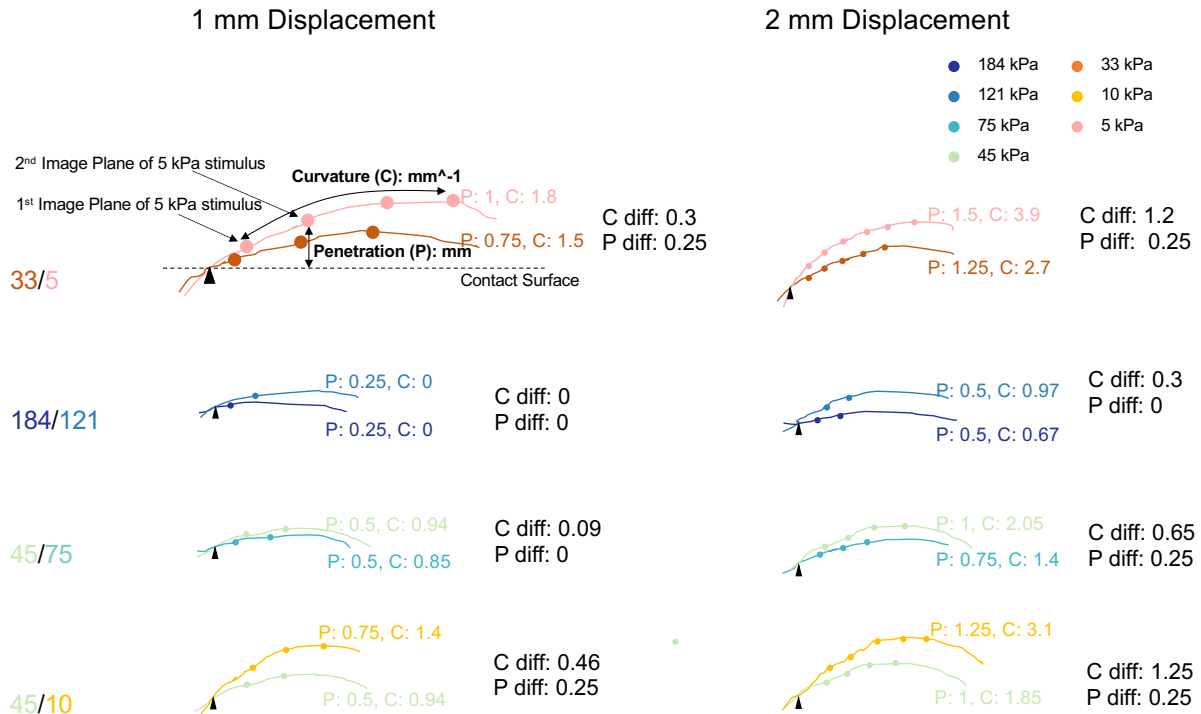


**Figure 5.** A cross-sectional contour representing an example participant’s deformed skin surface is overlaid with points of intersection obtained separately via the ellipse method fitted to the 3-D point cloud.

intersection of each image plane matches with the shape of contour lines and the difference between curvature and penetration depth cues reflects the discriminability for each stimulus pair.

*F. Summary.* Our results show that the discriminability of compliance is inversely proportional to the indentation rates for all stimulus comparisons, which may result from the insufficient time duration. For the developed cues, the recruitment of each cue depends on the surface compliance, time durations and indentation rates, however, all cues evolve complementarily in time courses to encode the perception of compliance. For example, people rely on penetration depth cue at first with an addition of contact area cue for the hard stimulus pair, whereas contact area cue appears to be the first for the soft pair then penetration depth cue. Fast indentation rates result in early statistical significance of each cue, but people cannot perceive the difference between stimuli during the experiments. The minimum time required to differentiate stimuli that are both harder and softer than skin is about 0.6 s. It takes less time for people to discriminate stimuli that is softer than skin (0.4 s) than harder than skin ( $> 2$ s).

## Methods and Materials

*A. Participants.* A total of 10 subjects (mean = 23, SD = 1.2, 6 male and 4 female) participated in psychophysical and biomechanical experiments. Experiments were conducted under an approved IRB protocol, with the informed consent for each participant. All devices were sanitized after each use, and participants wore facemasks, according to SARS-COVID-2 protocols. Participants are seated in a comfortable and adjustable chair with elbow resting on the desk throughout the duration of the experiment. The participant's forearm was placed on a customized stainless-steel support, at the angle of 30 degree with respect to the horizontal line. A plastic finger support is glued on the steel surface, which fixes the finger position and prevents unwanted movements during the experiment. An electrical-controlled indenter (ILS-100 MVTP, Newport, Irvine, CA) was used to vertically deliver a silicone stimulus into the center of the participant's index finger, with a preset indenting rate as shown in Figure 6A. An aluminum disk (radius = 50 mm, height = 20 mm) with silicone substrate was secured by a 3-D printed plastic cast that was mounted on an arm of the rotating wheel which was controlled by a servo motor. The rotating wheel has five arms in total and it is used to deliver the desired silicone stimulus vertically into the finger pad once at a time. The shifting time interval between two stimuli is less than 3 seconds which is short enough amount time for participants making judgements during the psychophysical experiments. Displacement in the Z-axis was controlled and measured by the cantilever attached to the indenter, and force was measured at the base of the silicone substrate holder by a load cell (LCFD-5, Omegadyne, Sunbury, OH) at 150 Hz. Two webcams (Papa look PA150, Shenzhen

Aoni Electronic Industry Co., Guangdong, China) are placed directly above the silicone stimulus and capture images at 30 frames per second. For more details about the apparatus setup, look at our previous work.

*B. Stimuli.* Seven silicone substrates with compliance scoped from 5 kPa to 184 kPa were used. The mean modulus of human skin on the fingertip is from 42 to 54 kPa [9]. We made one skin-like substrate with a modulus of 45 kPa, three substrates that are softer than the skin (5, 10, 33 kPa) and three harder-than-skin substrates (75, 121, 184 kPa). Later, we will compare the effects of changing substrate combinations on perceptual sensitivity to surface compliance. An aluminum container is made by sealing a clean, dry glass disc (2 x 0.125 inch) into a metal collar (2.125 inch) using a #18-gauge syringe tip filled with 0% diluted Solaris, heated in oven at 100 Celsius until it is fully sealed. The three softer-than-skin silicone substrates were made from two-component Solaris PDMS mixed with the desired dilution percentage with Silicone oil. Stir Solaris parts A and B individually and mix them together in a 1:1 ratio, then apply the appropriate amount of Silicone oil diluent (400% for 5 kPa, 300% for 10 kPa and 200% for 33 kPa) before pouring the mixture into the aluminum container. The stimulus assembly was rested under room temperature until all air bubbles have released, then cure it in oven at 100 Celsius for 25 minutes to let it fully solidify and cool it down under room temperature. To eliminate stickiness caused by high percentage of dilution, a layer of 100% diluted Solaris PDMS was applied to cover the entire surface of the substrate. Finally, the substrate with a layer of Solaris PDMS was cured under 100 Celsius for 15 minutes and cooled down to room temperature. The substrates that are harder than

skin (75, 121, 184 kPa) are the same as those used in the previous study (Bingxu, 2020). These substrates were made from two-component silicone rubber varying amounts of Silicone oil to achieve specimens of differing compliances.

*C. Biomechanical experiments.* The participant's index finger was secured by the customized plastic support and a thin layer of blue ink was applied on the skin surface using a paint brush. Seven stimuli ranging from 5 to 184 kPa were delivered to the center of the finger pad individually, under a displacement control up to 2 mm. Each stimulus was brought into the finger pad with a light contact force ( $< 0.1\text{N}$ ) before the indentation. Stimuli then were delivered at six rates of 1, 1.75, 2.5, 3.5, 4.5 and 6.5 mm/s and at displacements of 1, 2 mm without holding. The time duration of the loading phase ranges from 0.3 s (6.5 mm/s at 1 mm) to 2 s (1 mm/s at 2 mm) and the interval between each load was less than 3 seconds. In turn, each stimulus was indented into the finger pad at six rates and two displacements, repeated three times for each participant. There are 360 trails in total for the biomechanical experiments, including 6 indenting rates, 2 displacements, 3 repetitions and 10 participants. The average time to complete the experiment was about 70 minutes including 10-minute break after each trial.

*D. Psychophysical experiments.* Psychophysical experiments were conducted before the biomechanical experiments due to the higher demand of attention from participants. We prepared four pairs of stimulus comparison: 45/10 kPa, 184/121 kPa, 33/5 kPa and 45/75 kPa. We are able to examine the discriminability of compliance for the stimuli that are both harder and softer than the skin using 184/121 and 33/5 kPa pairs; Moreover, we can also detect the differential sensitivity of compliance by comparing the skin with softer and harder stimuli (45/10, 45/75 kPa). The

participant was seated on a comfortable chair and rested the index finger on the plastic support. All participants were blind folded to eliminate the visual cues. Each pair of stimulus comparison was delivered to the participant's finger pad sequentially, at the same rates and displacements as the biomechanical experiments. Each trail contains five randomized combinations of stimuli and the participants were asked to report which one of the two stimuli was softer. There are 400 trails in total including 2 stimuli in one pair, 4 pairs of comparison, 5 combinations and 10 participants. The average time for each participant was about 80 minutes including breaks.

*E. Data analysis.* Force, displacement and time duration were measured and plotted instantaneously using Python 3.6. The displacement was constant during the loading and unloading phases, but because the ramping rates were differed from 1 to 6.5 mm/s, the time duration increased from 0.3 s to 2 s. Images of the finger pad were captured by the left and right cameras every 0.1 s, then stored for later image processing procedure.

1) 3-D Surface Reconstruction and Image Processing. The disparity-mapping approach, previously defined [3] was used to generate a 3-D point cloud data that represents the deformation of the finger pad. The point cloud was obtained by co-locating the ink points on the skin surface and the identified pixel brightness values between left and right images are the coordinates of the points in 3-D domain. For the noise reduction, we firstly filtered out the high-frequency noise which could be caused by the lighting around the device, then manually extract the area that the skin and the stimulus making contact by masking the remaining areas, shown in Figure 6B - D. On average, each 3-D point cloud contains about 80,000 discrete points after noise reduction. We applied these two steps (filtering and masking) for each image frame to make sure the data was within the region of interest.

2) Ellipse Method and Image Planes To characterize the geometric change of the skin surface over the course of an indentation, we developed a method to fit the 3-D point cloud into vertically stacked ellipses that have the same orientation. We defined each ellipse as an image plane and each ellipse contains at least 98% of points per image plane with 95% confidence. With the procedure, first ellipse was fitted at the bottom which representing the contacting surface between the finger pad and the substrate, and the next ellipse was fitted upwards sequentially at an increment of 0.25 mm until the algorithm failed. The first image plane was defined to be the ellipse with deepest penetration while the last image plane represents the contact surface as illustrated in Figure 6F, G. We selected 0.25 mm as the increment value as it is as twice as the resolution of the stereo images in the vertical dimensions. The benefits of this ellipse representation are the dimensionality reduction and data denoising, composing 80,000 discrete points into a number of ellipses.

3) Dependent Metrics. We used the same metrics as defined in our previous work [10] to characterize the deformation of the skin's surface. *Penetration depth ( $P$ )* is defined as the distance between the first and last image plane, in units mm, is calculated as follows, where  $N$  is number of image planes. The reference is the surface contact plane.

*Curvature* is the average slope change between two adjacent image planes. It is estimated by the slope between two adjacent ellipses using their radius and the distance between them, with the resultant discrete slope values averaged across all ellipses for that point cloud, as follows, where  $r$  is the radius and  $i$  is the image plane. The radius represents the major axis of the ellipse, and all

ellipses are oriented in the same direction. The average slope approximates the 3-D curvature change of the point cloud as calculated in Equation (2).

$$P = (N - 1) * 0.25 \text{ -----(1)}$$

$$Slope_{ave} = \frac{\sum_{i=1}^{i=Nr(i+1)-r(i)} r(i)}{r(i)} \text{ -----(2)}$$

*Contact Area* is the last image plane formed on the contact surface and *Force* is measurement from the load cell. Figure 6E shows the development of the dependent metrics over time when the finger pad was indented by hard and soft substrates.

*F. Statistical analysis.* All image processing procedures were performed using MATLAB Computer Vision Toolbox and all data analysis were processed using Python 3.6. One-way ANOVA was used to establish the differences between stimuli for each cue and p-value of 0.05 is the threshold for statistical significance. The ANOVA test was applied to four pairs of stimulus comparison using four developed cues at each 0.1 second time interval across six indentation velocities. Table 1 shows an example of ANOVA test of four stimulus comparisons at 0.4 second under 6.5 mm/s indentation rate using force cue (Figure 2K). 184/121 kPa and 45/10 kPa stimulus comparisons were statistically significant ( $F = 3792.4$ ,  $p = 0.01$  and  $F = 1954.7$ ,  $p = 0.04$ ) while 33/5 kPa and 45/75 kPa were not differentiable ( $F = 13.9$ ,  $p = 0.79$  and  $F = 15.65$ ,  $p = 0.6$ ).

**Table 1:** ANOVA table of stimulus comparisons at 6.5 mm/s indentation velocity at 0.4 s using force cue.

Comparison Pairs (kPa)	df	Sum_sq	Mean_sq	F_value	PR(>F)
184/121	1.0	10426.7	10426.7	3792.4	0.01
33/5	1.0	1762	1762	13.91	0.79
45/10	1.0	9624.2	9624.2	1954.7	0.04
45/75	1.0	2564.3	2564.3	15.65	0.6
Residuals	104.0	1124.75	10.81	NaN	NaN

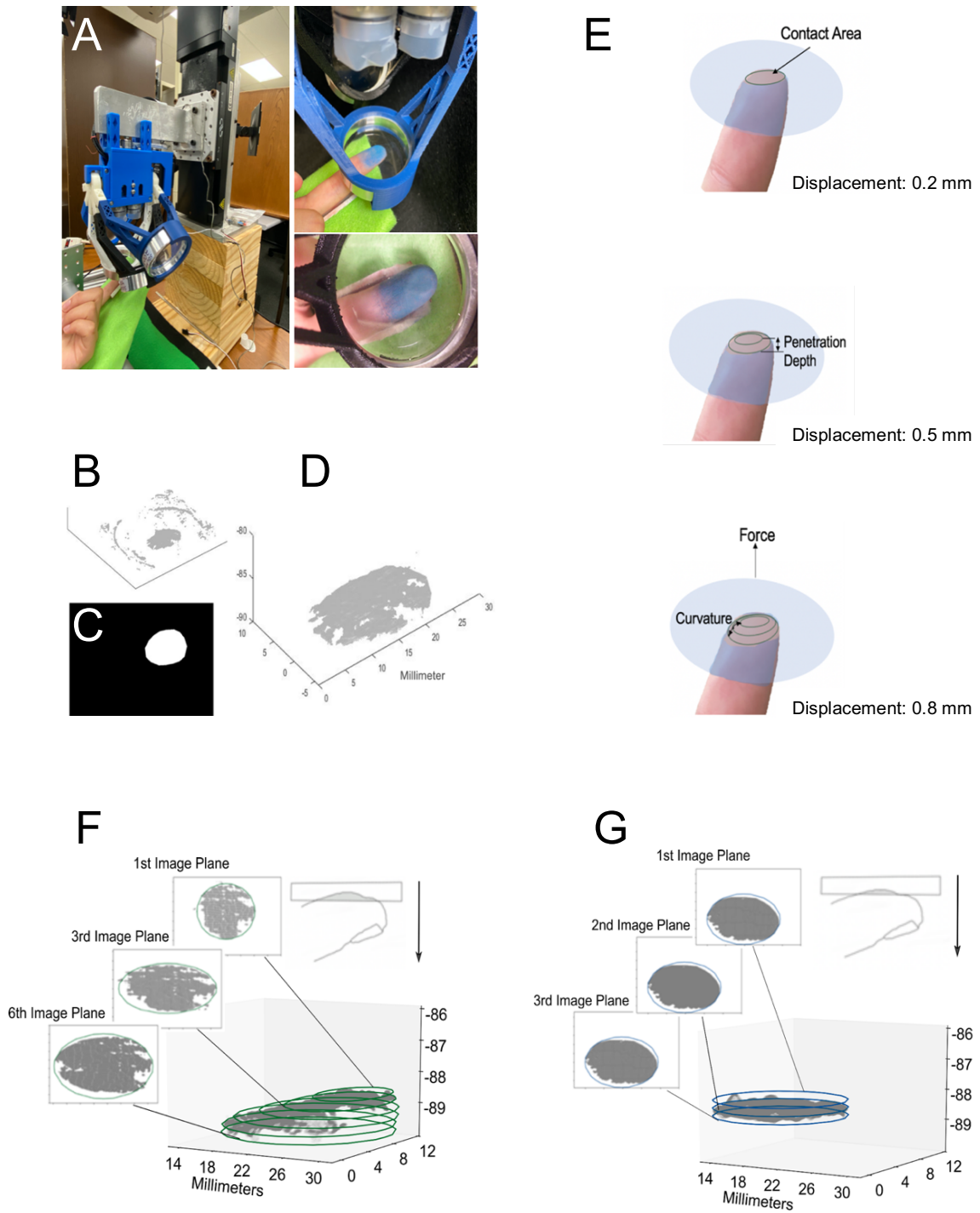


**Figure 6.** Procedure to obtain 3-D point clouds representing the skin deformation at the fingertip while being indented with soft and hard stimuli.

## Discussion

The aim of this study is to quantify the geometric deformation caused by surface compliance in human finger pad and connect the skin mechanics with human perception of compliance. The developed cues such as penetration depth and curvature were validated visually and statistically to describe the shape of fingertip under different compliant stimuli at any given time, shown in Figure 6. We have shown that the change of indenting rates influences both skin deformation and human perception, suggesting that higher indenting rates result in more dramatic geometric change on the skin surface while is not positively correlated to the differentiating sensitivity by human. As studied by Srinivasan and LaMotte, our experimental results agreed that the indenting rates have the ability to alter both skin deformation and human perception, which potentially can be used for creating compliance illusions.

*A. Usability of the developed cues.* We tested four developed cues under seven compliant stimuli at six indenting rates. The results show that curvature cue has the most sensitivity to differentiate compliance between stimuli. Force cue is only sensitive to higher indenting rates and stiffer stimuli. Contact area cue requires longer time duration to discriminate compliance whereas penetration cue takes less time but is not differentiable through the whole period. Based on its sensitivity, curvature cue can be potentially used to stimulate haptic feedback in engineering designs in addition to force and vibration controls [11][12][13]. Owing to its differentiating acuity using least time, penetration cue can also be a good candidate to the time-sensitive systems, such as surgical equipment and detecting sensors [14][15].

*B. Human discriminability to surface compliance.* In this study, we examine the differential sensitivity to compliant objects by varying the modulus and the indenting rate of the stimuli. The large tested range of compliance (three softer than the skin, one the same as the skin and three harder than the skin) and indenting rates (three fast and slow velocities) give us a good understanding of human perception of object compliance. The results indicate that it is easier for people to differentiate compliance that is softer than the skin compared to the stimuli that is stiffer than the skin, and the discriminability is almost the same for the stimuli that are both harder and softer than the skin. Interestingly, even though the higher indenting rates cause a more dramatic skin change, the discriminability decreases with the reduced time duration. Thus, we compared the discriminability with three levels of time duration and the results agreed that for the same time duration, the discriminability was almost the same. From the psychophysical results, the minimum amount of time required to differentiate between stimuli were determined: 0.56 s to differentiate 184/121 and 33/5 kPa pairs, and 0.3 s for 45/10 kPa pair. As it takes more time for people to differentiate objects in passive touch, it would be interesting to compare the detection time with active touch. The discrepancy of tactile sensitivity between psychophysical and biomechanical results shown in Figure 3 supports the theory that the subjects' detection threshold is higher than the threshold of their sense organs claimed by psychophysicists [16].

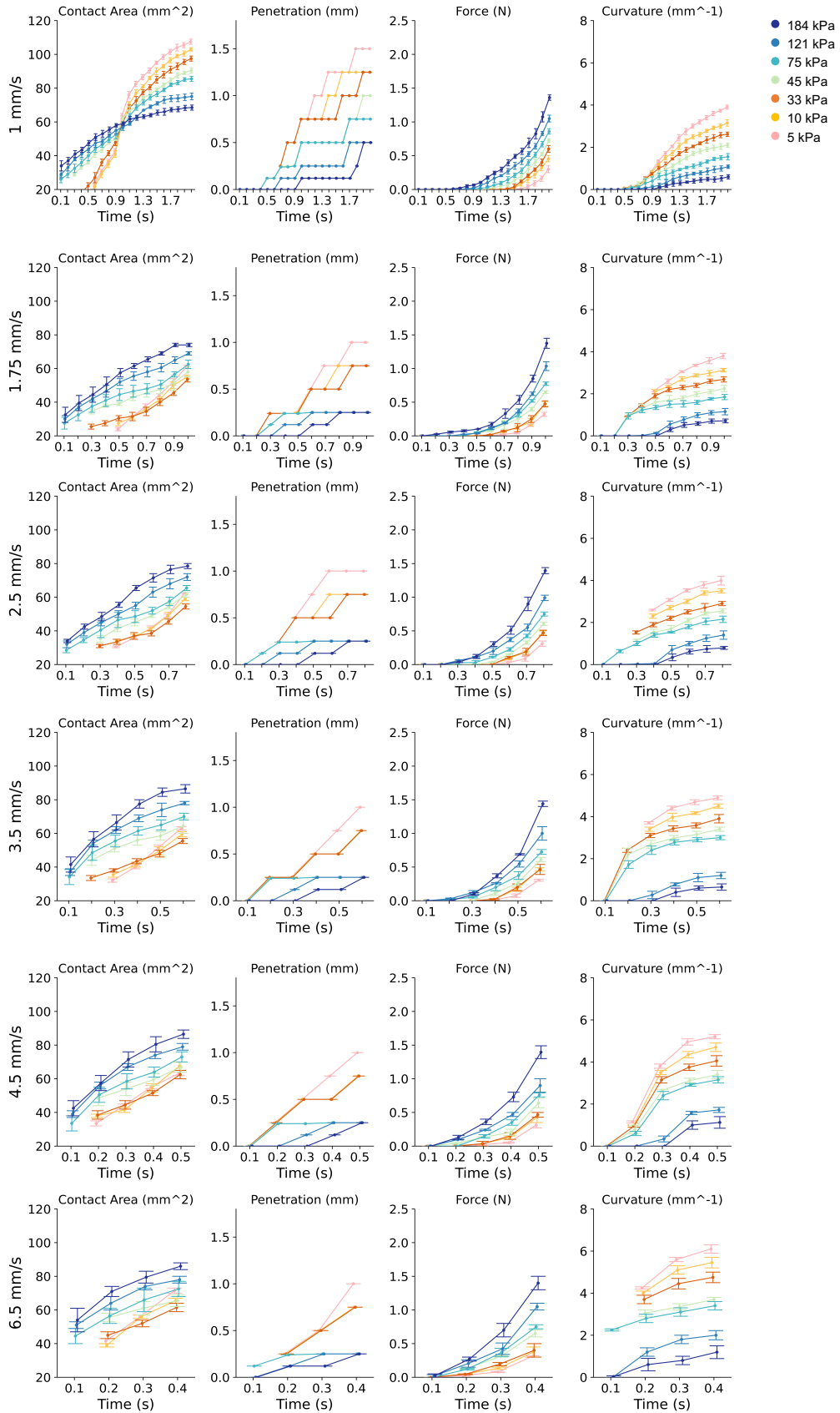
*C. Connections between cues and tactile afferents.* During the indenting process, the developed cues evolve in a complementary way in terms of the differentiating timing and differentiating duration. For example, penetration cue has the earliest differentiating timing but with the least differentiating duration. Each developed cue provides independent information about the geometric deformation of the skin. In neurology, Hannes and Sethu (2009) also found a similar

complementary role played by two firing properties, spiking timing and spike counts, of the SAI afferent, contributed independently to encode object curvatures and force directions. Based on this similarity, we hypothesize putative connections between the cutaneous cues and the tactile afferent activities, to map the skin mechanics to neuron responses. There are four neuron codes that could underlie perception: the spike counts, mean firing rate, spatial variation and first spike latency. Based on the existed neuroscience study, the force cue is correlated with the total number of active fibers [17] across the afferent unit. From the definition of contact area and curvature cues, we presume those two cues are corresponding to the spatial variation across the contact surfaces. Since penetration cue depicts how much the skin penetrates into the stimuli, it somehow explains the intensive recruitment of the afferents. And the indenting rates of stimuli directly affect the time duration which may have impact on the timing of afferent discharges. To validate those putative connections, more work should be done to track afferent responses and their firing properties under specific circumstances.

## References

- [1] M. C. Lin and M. A. Otaduy, *Haptic rendering: Foundations, algorithms, and applications*. 2008.
- [2] B. M. Dzidek, M. J. Adams, J. W. Andrews, Z. Zhang, and S. A. Johnson, “Contact mechanics of the human finger pad under compressive loads,” *J. R. Soc. Interface*, 2017.
- [3] S. C. Hauser and G. J. Gerling, “Imaging the 3-D deformation of the finger pad when interacting with compliant materials,” in *IEEE Haptics Symposium, HAPTICS*, 2018, vol. 2018-March, pp. 7–13.
- [4] M. A. Srinivasan and R. H. LaMotte, “Tactual discrimination of softness,” *J. Neurophysiol.*, vol. 73, no. 1, pp. 88–101, 1995.
- [5] K. O. Johnson and S. S. Hsiao, “Neural mechanisms of tactual form and texture perception,” *Annual Review of Neuroscience*. 1992.
- [6] S. J. Bensmaia and M. Hollins, “The vibrations of texture,” *Somatosens. Mot. Res.*, 2003.
- [7] G. A. Gescheider, S. J. Bolanowski, J. V. Pope, and R. T. Verrillo, “A four-channel analysis of the tactile sensitivity of the fingertip: Frequency selectivity, spatial summation, and temporal summation,” *Somatosens. Mot. Res.*, 2002.
- [8] G. A. Gescheider, J. H. Wright, and R. T. Verrillo, *Information-processing channels in the tactile sensory system: A psychophysical and physiological analysis*. 2008.
- [9] E. Miguel *et al.*, “Characterization of nonlinear finger pad mechanics for tactile rendering,” in *IEEE World Haptics Conference, WHC 2015*, 2015.
- [10] B. Li, S. Hauser, and G. J. Gerling, “Identifying 3-D spatiotemporal skin deformation cues evoked in interacting with compliant elastic surfaces,” in *IEEE Haptics Symposium, HAPTICS*, 2020.
- [11] H. Kim, M. Kim, and W. Lee, “HapThimble: A wearable haptic device towards usable virtual touch screen,” in *Conference on Human Factors in Computing Systems - Proceedings*, 2016.
- [12] L. Kim, P. Castillo, S. Follmer, and A. Israr, “VPS Tactile Display: Tactile Information Transfer of Vibration, Pressure, and Shear,” *Proc. ACM Interactive, Mobile, Wearable Ubiquitous Technol.*, 2019.
- [13] L. Zhu *et al.*, “Feel the inside: A haptic interface for navigating stress distribution inside objects,” *Vis. Comput.*, 2020.
- [14] C. H. King, M. O. Culjat, M. L. Franco, J. W. Bisley, E. Dutson, and W. S. Grundfest, “Optimization of a pneumatic balloon tactile display for robot-assisted surgery based on human perception,” *IEEE Trans. Biomed. Eng.*, 2008.
- [15] M. E. H. Eltaib and J. R. Hewit, “Tactile sensing technology for minimal access surgery - A review,” *Mechatronics*. 2003.
- [16] A. B. Vallbo and R. S. Johansson, “Properties of cutaneous mechanoreceptors in the human hand related to touch sensation,” *Hum. Neurobiol.*, 1984.
- [17] H. P. Saal, S. Vijayakumar, and R. S. Johansson, “Information about complex fingertip parameters in individual human tactile afferent neurons,” *J. Neurosci.*, 2009.

# Appendix 1: Biomechanical results for all indentation velocities



## Appendix 2: Ellipse Method and Generated cues

```
import numpy
import pandas as pd
import matplotlib
matplotlib.use("TkAgg")
from matplotlib import pyplot as plt
from mpl_toolkits.mplot3d import Axes3D
from matplotlib.patches import Ellipse

def fitEllipse(cont, ell_coord):
    x = cont['X']
    y = cont['Y']

    x = x[:, None]
    y = y[:, None]

    D = numpy.hstack([x * x, x * y, y * y, x, y, numpy.ones(x.shape)])
    S = numpy.dot(D.T, D)
    C = numpy.zeros([6, 6])
    C[0, 2] = C[2, 0] = 2
    C[1, 1] = -1
    E, V = numpy.linalg.eig(numpy.dot(numpy.linalg.inv(S), C))
```

```

# if method==1:

n = numpy.argmax(numpy.abs(E))

# else:

# n=numpy.argmax(E)

a = V[:, n]

# -----Fit ellipse-----

b, c, d, f, g, a = a[1] / 2., a[2], a[3] / 2., a[4] / 2., a[5], a[0]

num = b * b - a * c

cx = (c * d - b * f) / num

cy = (a * f - b * d) / num

angle = 0.5 * numpy.arctan(2 * b / (a - c)) # *180/numpy.pi

up = 2 * (a * f * f + c * d * d + g * b * b - 2 * b * d * f - a * c * g)

down1 = (b * b - a * c) * ((c - a) * numpy.sqrt(1 + 4 * b * b / ((a - c) * (a - c))) - (c + a))

down2 = (b * b - a * c) * ((a - c) * numpy.sqrt(1 + 4 * b * b / ((a - c) * (a - c))) - (c + a))

a = numpy.sqrt(abs(up / down1))

b = numpy.sqrt(abs(up / down2))

area = numpy.pi * a * b

# print(area)

# print("majoraxis=",a)

# print("center=",cx,cy)

```

```

# -----Get path-----

ell = Ellipse((cx, cy), a * 3, b * 3, angle)

ell_coord = ell.get_verts()

params = [cx, cy, a, b, angle]

return params, ell_coord, area, a, b

def xy_from_ellipse(xcent, ycent, a, b, phi): #needed to plot the ellipse in matplotlib

    R = numpy.linspace(0,2*numpy.pi,100)

    xx = cx + a*numpy.cos(R)*numpy.cos(phi) - b*numpy.sin(R)*numpy.sin(phi)

    yy = cy + a*numpy.cos(R)*numpy.sin(phi) + b*numpy.sin(R)*numpy.cos(phi)

    return xx,yy

def plotConts(contour_list,idx, color,alpha):

    x = []

    y = []

    #fig = plt.figure()

    # ax = fig.add_subplot(111, projection='3d')

    for ii,cii in enumerate(contour_list):

        x.append(cii[1])

        y.append(cii[0])

    ax.plot(y,x,idx, color,alpha)

```

```

#ax.set_zlim([-91,-89])

ax.grid(False)

df = pd.read_csv('/Users/bingbing/Desktop/Ellipse code/0.1s2mm/BX-35-A-0.5mms-
0.6S.csv')

df.dropna(inplace=True)

df.columns = ['X','Y','Z']

x= df['X']

y= df['Y']

z = df['Z']

### Make plots

fig = plt.figure()

ax = fig.add_subplot(122, projection='3d')

ax.plot(x,y,z,'.',alpha = 0.5,markersize = 0.2,color="gray")

# Only pointcloud

ax2 = fig.add_subplot(121,projection='3d')

ax2.plot(x,y,z,'.',alpha = 0.5,markersize = 0.2,color="gray")

ax2.grid(False)

#ax2.set_zlim([-92,-87])

def on_move(event):

```

```

if event.inaxes == ax:
    ax2.view_init(elev=ax.elev, azim=ax.azim)
elif event.inaxes == ax2:
    ax.view_init(elev=ax2.elev, azim=ax2.azim)
else:
    return
fig.canvas.draw_idle()

```

```
c1 = fig.canvas.mpl_connect('motion_notify_event', on_move)
```

```
lowb = -91
```

```
increment = 0.25
```

```
arealist=[]
```

```
count = 0
```

```
for i in range(0,10):
```

```
    lowb = lowb + increment
```

```
    filt = df['Z'] > lowb
```

```
    data = df.loc[filt,['X','Y']]
```

```
    #print(data.shape)
```

```
    _,ell2,area,a,b = fitEllipse(data,2)
```

```
    arealist.append(area)
```

```
    penetration=(len(arealist)-1)*increment
```

```
if arealist[i] < arealist[i-1] and 2*arealist[i] > arealist[i-1]: #2*arealist[i] > arealist[i-1]
```

```
# Plot ellipses
```

```
plotConts(ell2, lowb, color='#006d2c',alpha=0.3)
```

```
#print(arealist)
```

```
else:
```

```
#print("jj")
```

```
count+=1
```

```
if count == 2:
```

```
break
```

```
#print(arealist)
```

```
#print(penetration)
```

```
plt.show()
```

```
# save contact area and penetration in dataframe
```

```
data = pd.DataFrame({'kpa': [], 'Time': [], 'Area': [], 'Penetration': []})
```

```
for i in range(0,len(arealist)-1):
```

```
    kpa = 121
```

```
    Area = arealist[i]
```

```
Penetration = 0.25*(i)
```

```
Time = 0.1
```

```
data=data.append({'kpa':kpa,
```

```
    'Time':Time,
```

```
    'Area':Area,
```

```
    'Penetration':Penetration},ignore_index=True
```

```
)
```

```
print(data)
```

```
#data.to_csv('data_121kpa_0.5mm.csv', index=False)
```

```
#data.to_csv('data_121kpa_0.5mm.csv', header=False,mode='a',index=False)
```

### Appendix 3: Plotting for the developed cues

```
import numpy
import pandas as pd
import matplotlib
matplotlib.use("TkAgg")
from matplotlib import pyplot as plt
import seaborn as sns

### Colors

# 45kpa: #c7e9b4
# 75kpa: #41b6c4
# 121kpa: #2c7fb8
# 184kpa: #253494

fig, axes = plt.subplots(1, 4, figsize=(12, 4))
plt.subplots_adjust(left=0.06, bottom=0.18, right=0.96, top=0.86, wspace=0.3, hspace=0.2)
color = ['#fbb4b9', '#fec44f', '#d95f0e', '#c7e9b4', '#41b6c4', '#2c7fb8', '#253494']
#color = ['#253494', '#2c7fb8', '#41b6c4', '#c7e9b4', '#fec44f', '#d95f0e', '#fbb4b9']

df_45 = pd.read_csv('4.5mms.csv')
```

```

Time = df_45['Time']
Area_45 = df_45['Area']
Pene_45 = df_45['Penetration']
force_45 = df_45['Force']
Cur_45 = df_45['Curvature']

ax1 = sns.pointplot(x="Time", y="Area", hue="kpa", data=df_45, palette=color, markers='o',
                    scale = .4, ci=95, capsize=.4, dodge=True, errwidth=1,
                    ax=axes[0])
ax1.set_title('Contact Area (mm^2)', fontsize=14)
ax1.set_xlabel('Time (s)', fontsize=16)
ax1.set_ylabel('4.5 mm/s', fontsize=18)
ax1.set_ylim(20, 120)
ax1.tick_params(axis = 'both', which = 'major', labelsize = 14)
for ind, label in enumerate(ax1.get_xticklabels()):
    if ind % 10 == 0: # every 10th label is kept
        label.set_visible(True)
    else:
        label.set_visible(False)

ax1.get_legend().remove()

```

```

ax1.spines['top'].set_visible(False)

ax1.spines['right'].set_visible(False)

#ax1.legend(numpoints=1, loc=2, scatterpoints=1, frameon=False)

#

#

ax2 = sns.pointplot(x="Time", y="Penetration", hue="kpa", data=df_45,
palette=color, markers='o',
                    scale = .4, ci=95, capsize=.4, dodge=True, errwidth=1,
                    ax=axes[1])

ax2.set_title('Penetration (mm)', fontsize=14)

ax2.set_ylabel("")

ax2.set_xlabel('Time (s)', fontsize=16)

ax2.set_ylim(0, 1.8)

ax2.tick_params(axis = 'both', which = 'major', labelsize = 14)

for ind, label in enumerate(ax2.get_xticklabels()):

    if ind % 10 == 0: # every 10th label is kept

        label.set_visible(True)

    else:

        label.set_visible(False)

ax2.get_legend().remove()

ax2.spines['top'].set_visible(False)

```

```

ax2.spines['right'].set_visible(False)

#ax2.legend(numpoints=1, loc=2, scatterpoints=1, frameon=False)

ax3 = sns.pointplot(x="Time", y="Force", hue="kpa", data=df_45, palette=color, markers='o',
                    scale = .4, ci=95, capsize=.4, dodge=True, errwidth=1,
                    ax=axes[2])

ax3.set_title('Force (N)', fontsize=14)

ax3.set_ylabel("")

ax3.set_xlabel('Time (s)', fontsize=16)

ax3.set_ylim(0, 2.5)

ax3.tick_params(axis = 'both', which = 'major', labelsize = 14)

for ind, label in enumerate(ax3.get_xticklabels()):

    if ind % 10 == 0: # every 10th label is kept

        label.set_visible(True)

    else:

        label.set_visible(False)

ax3.get_legend().remove()

ax3.spines['top'].set_visible(False)

ax3.spines['right'].set_visible(False)

##

##

##

ax4 = sns.pointplot(x="Time", y="Curvature", hue="kpa", data=df_45,

```

```

palette=color,markers='o',

    scale = .4,ci=95,capsize=.4,dodge=True,errwidth=1,

    ax=axes[3])

ax4.set_title('Curvature (mm-1)',fontsize=14)

ax4.set_ylabel("")

ax4.set_xlabel('Time (s)',fontsize=16)

ax4.tick_params(axis = 'both', which = 'major', labelsize = 14)

ax4.set_ylim(0,8)

for ind, label in enumerate(ax4.get_xticklabels()):

    if ind % 10 == 0: # every 10th label is kept

        label.set_visible(True)

    else:

        label.set_visible(False)

ax4.get_legend().remove()

plt.legend()

ax4.spines['top'].set_visible(False)

ax4.spines['right'].set_visible(False)

plt.rcParams["axes.labelsize"] = 20

plt.rcParams["font.family"] = "Arial"

plt.rcParams["axes.formatter.useoffset"] = False

plt.autofmt_xdate()

```

```
plt.show()
```

```
#fig.savefig('4.5 mms.png', bbox_inches='tight', dpi=1200)
```

## Appendix 4: The image processing algorithm

%with the disparity map, and the stereo parameters, we can reconstruct

%the 3D points.

```
load('calibration_2019-05-22_14-40-08.mat');
```

```
drange = [348, 444];
```

```
factor = .95;
```

```
left = imread('left0003.png');
```

```
right = imread('right0003.png');
```

```
outputsize = ceil(factor*size(left(:,:,1))));
```

```
left_resize = imresize(left,factor,'outputsize',[outputsize]);
```

```
left_resize = padarray(left_resize,(size(left(:,:,1))-outputsize)/2);
```

```
right_resize = imresize(right,factor,'outputsize',[outputsize]);
```

```
right_resize = padarray(right_resize,(size(right(:,:,1))-outputsize)/2);
```

```
[lrect,rrect]=rectifyStereoImages(left_resize,right_resize,stereoParams);
```

```
I = lrect;
```

```
lrect=double(lrect);
```

```
rrect=double(rrect);
```

```

I1_L = (lrect(:,:, 1)+lrect(:,:, 2)+lrect(:,:, 3))./ 3. / 255;
I1_R = (rrect(:,:, 1)+rrect(:,:, 2)+rrect(:,:, 3))./ 3. / 255;

dMap_raw =
disparity(I1_L,I1_R,'DisparityRange',drange,'BlockSize',11,'uniquenessthreshold',20);

pts3D = reconstructScene(dMap_raw, stereoParams); % the 3-D points are generated
pc = pointCloud(pts3D,'color',lrect./255); % puts it in a matlab cloud object
pRGB = pc.Color;
pL = pc.Location;

XYZ = pL;
pX = XYZ(:,:,1); pY = XYZ(:,:,2); pZ = XYZ(:,:,3);

% comment this back on to select a new region.
%figure; imagesc(I); roipoly;

poly = [817.685483870968 238.357142857143;855.157834101383
195.639941690962;912.807603686636 164.572886297376;993.517281105991
156.80612244898;1033.87211981567 187.873177842565;1051.16705069124
236.415451895044;1033.87211981567 296.607871720117;979.104838709678
343.208454810496;892.630184331797 358.741982507289;829.215437788019
327.674927113703;803.273041474655 286.899416909621]

```

```

msk = poly2mask(poly(:,1), poly(:,2), size(I,1),size(I,2));

% get just the X,Y,Z in the mask area that you want

msk_indices = find(msk);

XYZ_msk = [pX(msk_indices),pY(msk_indices),-pZ(msk_indices)];

figure;subplot(4,1,1); imshow(I);

subplot(4,1,2);

plot3(reshape(XYZ(:,1),[],1), reshape(XYZ(:,2),[],1), -
reshape(XYZ(:,3),[],1),'b','markersize',.2);

zlim([-90,-80]); daspect([1 1 1]);

subplot(4,1,3); imshow(msk);

subplot(4,1,4); plot3(XYZ_msk(:,1), XYZ_msk(:,2), XYZ_msk(:,3),'g','markersize',.2);

zlim([-90,-80]); daspect([1 1 1]);

%figure;imshow(I);

%plot3(reshape(XYZ(:,1),[],1), reshape(XYZ(:,2),[],1), -
reshape(XYZ(:,3),[],1),'!','markersize',.2,'Color',[0.7,0.7,0.7]);zlim([-90,-80]); daspect([1 1
1]);set(gca,'xtick',[],'ytick',[],'ztick',[]);

```

```
%figure(2);imshow(msk);  
  
%figure(3);plot3(XYZ_msk(:,1), XYZ_msk(:,2),  
XYZ_msk(:,3),'.','markersize',.2,'Color',[0.7,0.7,0.7]);  
  
%ax = gca;  
  
%ax.XAxis.FontSize = 17;  
  
%ax.YAxis.FontSize = 17;  
  
%ax.ZAxis.FontSize = 17;  
  
%zlim([-90,-80]);  
  
%daspect([1 1 1],xlabel('Millimeters','fontsize',20));  
  
%xlabel('Millimeters','fontsize',20);
```